Phonons in zinc-blende and wurtzite phases of GaN, AlN, and BN with the adiabatic bond-charge model

H. M. Tütüncü[1] and G. P. Srivastava[2]
[1]*Sakarya Üniversitesi, Fen-Edebiyat Fakültesi, Fizik Bölümü, Adapazarı, Turkey*
[2]*School of Physics, University of Exeter, Stocker Road, Exeter EX4 4QL, United Kingdom*
(Received 24 January 2000)

The lattice dynamics of the zinc-blende and wurtzite phases of GaN, AlN, and BN is studied using the adiabatic bond-charge model. The resulting phonon spectra for zinc-blende GaN and AlN compare very well with *ab initio* calculations along symmetry directions. We discuss the effect of the internal parameter u on the A_1(LO) and E_1(LO) modes. We also present the angle dependence of the zone-center optical-phonon modes in the wurtzite phase. The anticrossing behavior of the A_1 acoustic and E_2 optical modes is also discussed.

I. INTRODUCTION

Recently, the Group-III nitrides have been among the most widely studied semiconductors because of their important device applications. For example, these materials can be used for short-wavelength electroluminescence devices and high-temperature, high-power, and high-frequency electronics. It is well known that many properties inherent to device performance, such as thermodynamic and transport properties, are strongly dependent on the lattice-dynamical characteristics. The Group-III-N compounds exist in both zinc-blende (ZB) and wurtzite (WZ) phases, and it is therefore important to obtain a full understanding of the lattice dynamics of both phases.

In general, two widely used experimental techniques to study phonon modes in bulk solids are inelastic neutron scattering and Raman scattering. Due to difficulty in preparing large Group-III–N single crystals the inelastic neutron scattering technique has not yet been successfully applied. The first-order Raman-scattering technique provides information about selected phonon modes at the zone center. In contrast, second-order Raman scattering experiments can provide information regarding phonon modes throughout the Brillouin zone, but so far there is no report of the full vibrational spectrum using this technique. Measurements of zone-center and zone-boundary phonon modes, using the Raman scattering techniques, in ZB and WZ phases of GaN and AlN have been presented by several groups.[1–11] Recently, the phonon-dispersion data in hexagonal AlN have been obtained with inelastic x-ray scattering measurements.[12]

Theoretical investigations of the lattice dynamics of these materials have been made by using a variety of methods, including a two parameter Keating model,[13] a valence-force model,[8] the rigid-ion model,[9] and *ab initio* calculations within the frozen phonon approach,[14–16] supercell approach,[17] and a linear-response approach.[12,18–21] While *ab initio* calculations are computationally very demanding, other approaches lack physical clarity. On the other hand, the adiabatic bond-charge model is based upon a clear physical appeal for the role played by valence electrons in tetrahedrally bonded materials, and has successfully been applied to a number of Group-IV, III–V, and II–VI semiconductors,[22] their surfaces,[23] and superlattices.[24] It is therefore expected that this method can be successfully applied to the investigations of the lattice dynamics in the ZB and WZ phases of Group-III–N materials.

In this paper we present an adiabatic bond-charge model study of the lattice dynamics of GaN, AlN, and BN semiconductors in both ZB and WZ structures. We provide a comparison of the phonon spectra for the ZB and WZ phases, and test our results against Raman measurements and existing *ab initio* calculations. The anisotropic behavior in the vibrational characteristics of the WZ structure is studied by discussing the angular dependence of some zone-center optical modes. We also discuss the effect of internal parameter u on the A_1(LO) and E_1(LO) frequencies. Finally, we discuss the anticrossing behavior of the A_1 acoustic and E_2 optical modes.

II. THEORY

A. An adiabatic bond-charge model for the zinc-blende structure

The adiabatic bond-charge model (BCM) is based on a representation of the valence electron charge density by means of massless point charges (BC's), which are allowed to move adiabatically following ionic displacement. The BC's are located midway between neighboring atoms for homopolar covalent crystals with the valence charge density showing strong maximum between two atoms. For Group-III–V zinc-blende semiconductors, the BC's are located between two atoms, dividing the bond in the ratio 3:5. Thus, the bond charge is located at $r_1 = r(1+p)/2$ from the cation and $r_2 = r(1-p)/2$ from the anion, with r as the bond length between nearest-neighbor ions. For diamond structure semiconductors, $p=0$ and for zinc-blende semiconductors $p=0.25$. In the application of the BCM, the two ionic charges in the primitive unit cell are assumed to be equal: these are taken as $Z_1 = Z_2 = -2Ze$, where Ze is the bond charge. The following interactions are considered:[22]

(a) *Central short-range interactions*: We consider a pair potential ϕ_{1-2} for the central interaction between nearest-neighbor ions, and pair potentials ϕ_{1-1} and ϕ_{2-2} for the central interaction between second nearest-neighbor ions,

TABLE I. BCM parameters for GaN, AlN, and BN, given in units of e^2/v_a, where v_a is the unit cell volume for the zinc-blende structure. Here $i1$ and $i2$ represent ions, with 1 for cation (Group-III element) and 2 for anion (N).

	$i1$-$i2$ ϕ''_{1-2}	$i1$-BC ϕ''_{1-BC}	$i2$-BC ϕ''_{2-BC}	BC-$i1$-BC B_1	BC-$i2$-BC B_2	$i1$-$i1$ ϕ''_{1-1}	$i1$-$i1$ ϕ'_{1-1}/r_{1-1}	$i2$-$i2$ ϕ''_{2-2}	Z^2/ε
GaN	24.00	2.60	175.0	0.10	70.00	2.50	−0.50	0.28	0.350
AlN	27.00	2.000	138.0	0.10	86.00	2.50	−0.35	0.10	0.350
BN	16.00	5.50	960.0	1.00	60.00	1.20	0.15	1.80	0.295

where 1 and 2 label the two types of ions. The interaction between nearest ion-BC pairs is considered via potentials ϕ_{1-BC} and ϕ_{2-BC}.

(b) *Bond-bending interactions*: Bond-bending interactions are taken into account by using the Keating potential. Any two BC's i,j, centered around a common ion σ, interact with each other and with the ion via a Keating potential

$$V_{bb}^{(\sigma)}=\tfrac{1}{2}B_\sigma(\mathbf{X}_{\sigma i}\mathbf{X}_{\sigma j}+a_\sigma^2)^2/4a_\sigma^2, \tag{1}$$

where B_σ are force constants, $\mathbf{X}_{\sigma i},\mathbf{X}_{\sigma j}$ are the distance vectors between ions σ ($\sigma=1,2$) and BC's i,j, and a_σ^2 is the equilibrium value of $-\mathbf{X}_{\sigma i}\mathbf{X}_{\sigma j}$.

(c) *Long-range interaction*: Long-range interaction between all particles are taken into account by using the Ewald lattice sum technique. This leads to a Coulomb dynamical matrix of size 18×18, corresponding to a total of 6 charged particles (2 ions and 4 BC's) in the primitive unit cell ($\alpha,\beta=x,y,z$):

$$C^C_{\alpha\beta}(bb';\mathbf{q})=\frac{e^2}{v_a}\frac{Z^2}{\varepsilon}\begin{bmatrix}4C_R & -2C_T\\ -2C_T^+ & C_S\end{bmatrix}, \tag{2}$$

where C_R, C_T, C_T^+, and C_S denote the ion-ion, ion-BC, BC-ion, and BC-BC Coulomb matrices, respectively, ε is the dielectric constant and v_a is the volume of the unit cell.

Considering the above interactions, the crystal energy per unit cell can be written in terms of the nearest-neighbor distance r as

$$E=4\phi_{i-i}+4\phi_{1-BC}+4\phi_{2-BC}+12\phi_{1-1}+12\phi_{2-2}+6[V_{bb}^1+V_{bb}^2]-\alpha_m\frac{4Z^2e^2}{\varepsilon r}, \tag{3}$$

where α_m is the Madelung constant. Using the equilibrium conditions

$$\left.\frac{\partial E}{\partial r}\right|_{r=r_0}=0$$

and

$$\frac{\partial E}{\partial p}=0,$$

and making the reasonable assumptions $(1+p)\phi'_{1-BC}-(1-p)\phi'_{2-BC}=0$ and $\phi'_{1-1}=-\phi'_{2-2}$, we can express

$$\phi'_{1-2}=-\frac{\alpha_m Z^2e^2}{\varepsilon r_o^2},$$

$$\frac{\phi'_{1-\mathrm{BC}}}{r_1}=\frac{2(1-p)}{(1+p)}\frac{\partial\alpha_m}{\partial p}\frac{Z^2e^2}{\varepsilon}\frac{1}{r_0^3},$$

$$\frac{\phi'_{2-\mathrm{BC}}}{r_2}=-\frac{2(1+p)}{(1-p)}\frac{\partial\alpha_m}{\partial p}\frac{Z^2e^2}{\varepsilon}\frac{1}{r_0^3}. \tag{4}$$

The values of α_m and $\partial\alpha_m/\partial p$ are determined to be 4.779 and 2.764, respectively. Thus in the present application of the BCM, we consider a total of nine adjustable parameters: ϕ''_{1-2}, $\phi''_{1-\mathrm{BC}}$, ϕ''_{1-1}, ϕ'_{1-1}, ϕ''_{2-2}, $\phi''_{2-\mathrm{BC}}$, B_1, B_2, and Z^2/ε. The derivatives ϕ' and ϕ'' are taken with respect to the nearest-neighbor distance r and evaluated at the equilibrium distance r_0. We choose these parameters to fit experimental LO and TO frequencies at Γ and *ab initio* results at the symmetry points K, X, and L. These parameters are listed in Table I.

B. Extension of the model for the wurtzite structure

For the wurtzite structure, we have considered the ideal value of the ratio c/a_{hex}. The internal atomic structural parameter u and the hexagonal lattice constant a_{hex} are taken from experimental results for GaN and AlN[25] and *ab initio* results for BN.[18] For this structure, the values of the parameters $\phi''_{1-\mathrm{BC}}$, ϕ''_{1-1}, ϕ'_{1-1}, ϕ'_{2-2}, $\phi''_{2-\mathrm{BC}}$, B_1, B_2, and Z^2/ε are considered to be the same as in the ZB structure, and we chose values of ϕ''_{1-2} by fitting the results for E_1(LO) and A_1(LO) to experimental or *ab initio* results. It should be mentioned that in this structure, ϕ''_{1-2} has two values [$\phi''_{1-2}(L)$ and $\phi''_{1-2}(S)$] for long and short bonds, respectively, as for values of $u>\frac{3}{8}$ the straight bond in the [111] direction is slightly longer than the other three

TABLE II. The lattice constant, internal parameter u, and additional force constants $\phi''_{1-2}(L)$ and $\phi''_{1-2}(S)$ for the wurtzite phase of GaN, AlN, and BN. The force constant parameters are in units of e^2/v_a^h, where v_a^h is the unit cell volume for wurtzite structure.

	a_{hex} (Å)	u	$\phi''_{1-2}(L)$	$\phi''_{1-2}(S)$
GaN	3.190[a]	0.377[a]	46.14	48.00
AlN	3.110[a]	0.382[a]	48.22	56.14
BN	2.531[b]	0.3751[b]	28.08	30.48

[a]Reference 25.
[b]Reference 18.

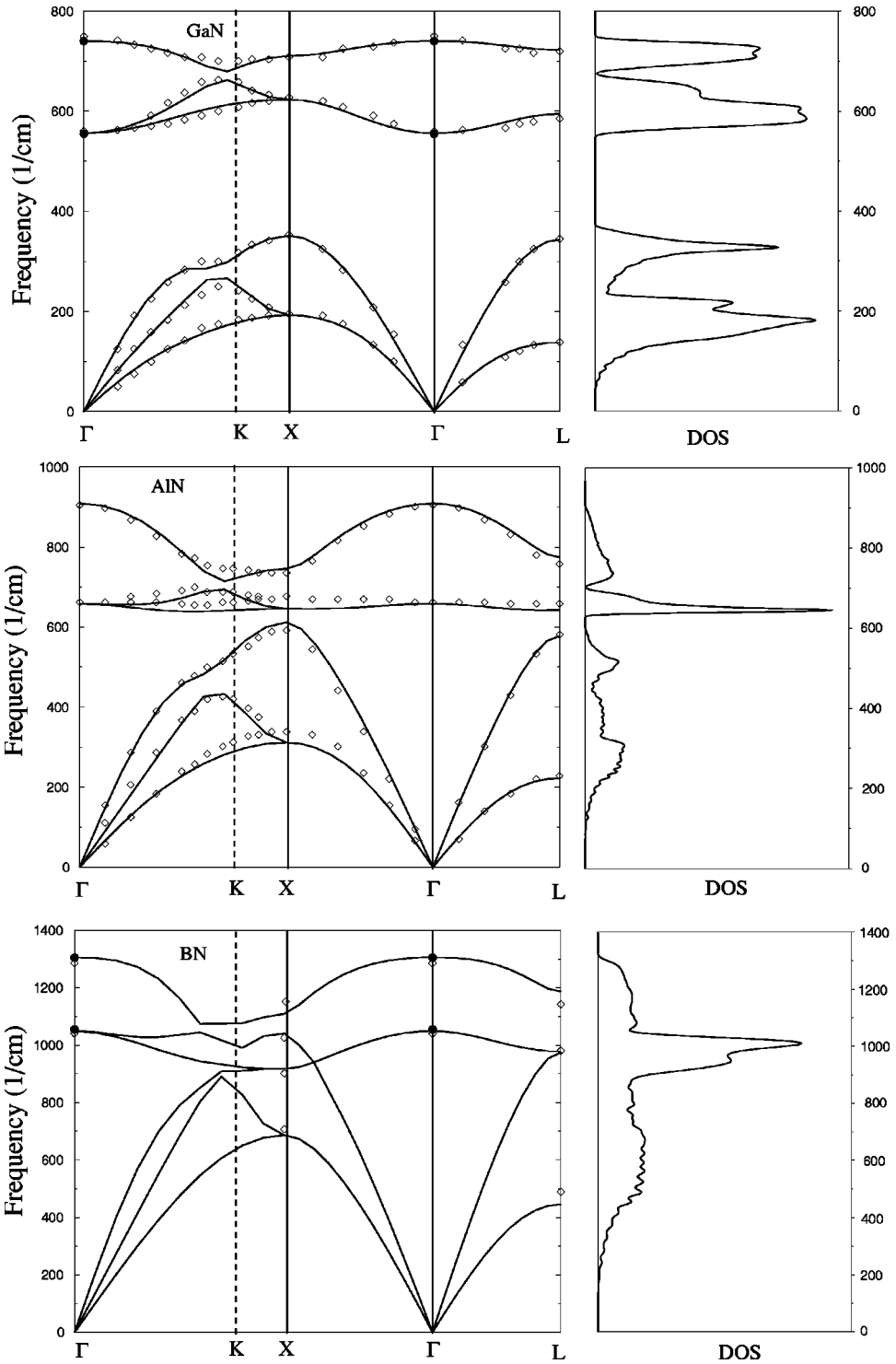

FIG. 1. Phonon-dispersion curves and phonon density-of-states for GaN, AlN, and BN in the zinc-blende structure. Open diamonds are taken from *ab initio* calculations (Refs. 18 and 19) while filled circles are experimental results from Ref. 7 for GaN and Ref. 26 for BN.

(slanted) bonds. Table II presents the values of $\phi''_{1-2}(L)$ and $\phi''_{1-2}(\mathrm{S})$ together with a_{hex} and u.

III. RESULTS

A. Zinc-blende structure

Figure 1 displays the phonon spectrum and density-of-states for zinc-blende GaN, AlN, and BN. The calculated results are shown by solid lines while *ab initio*[18,19] and experimental results[7,26] are shown by open diamonds and filled circles, respectively. Along the symmetry directions, our results are in very good agreement with the *ab initio* results.

In accordance with the decrease in the cation mass, the zone-boundary frequencies and the zone-center optical frequencies increase for the sequence GaN–AlN–BN. Similarly, in accordance with the increase in the anion/cation mass ratio, the optical-acoustic band gap decreases for the sequence GaN–AlN–BN. In fact, there is no optical-acoustic band gap for BN. The different degree of mixture of the ionic and covalent bondings in these materials results in different amounts of LO-TO splitting as well as different dispersion characteristics of the LO and TO modes. Some striking features are: (i) flatness of the TO branch in AlN, leading to a very sharp peak in the density-of-states, (ii) compared to

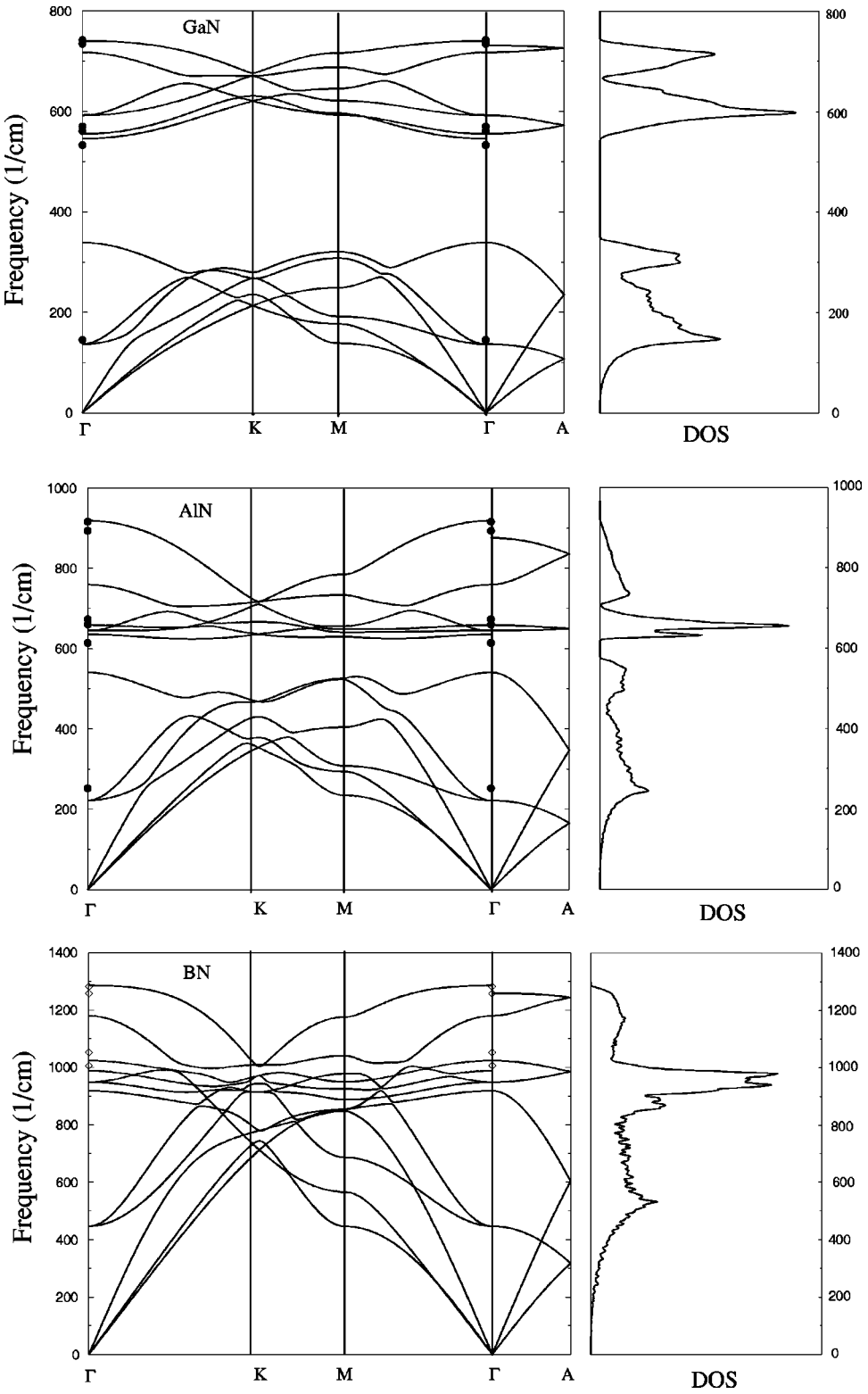

FIG. 2. Phonon-dispersion curves and phonon density-of-states for GaN, AlN, and BN in the wurtzite structure. Open diamonds are taken from *ab initio* calculations in Ref. 18, while filled circles are experimental results from Ref. 6 for GaN and Ref. 2 for AlN.

AlN and BN there is a shallower dispersion of the LO branch in GaN, leading to a clear LO peak in the density-of-states, and (iii) an upward dispersion of the TO branches in GaN. Finally, it is interesting to notice that, in both the acoustic as well as the optical frequency ranges, there is a gradual development of sharp density-of-states with distinct longitudinal and transverse peaks as we move along the sequence BN–AlN–GaN. For example, while there is only a broad feature in the acoustic range for BN, there are two distinct but small peaks for AlN, and there are at least two large and sharply defined peaks for GaN.

B. Wurtzite structure

The phonon dispersion curves and density-of-states of GaN, AlN, and BN in the wurtzite structure are shown in Fig. 2. Our results are in good agreement with experimental results for GaN[6] and AlN.[2,12] A comparison of presently cal-

TABLE III. The calculated zone center frequencies for wurtzite GaN, AlN, and BN and their comparison with experiments and available theoretical calculations. Units are cm^{-1}.

		E_2^1	B_1^1	A_1(TO)	E_1(TO)	E_2^2	B_1^2	A_1(LO)	E_1(LO)
GaN	This work	137	339	546	555	592	717	732	741
	Calc.[a]	146	335	534	556	560	697		
	Calc.[b]	150	330	537	555	558	677		
	Calc.[c]	143	337	541	568	579	720	748	757
	Calc.[d]	153	318	545	553	564	726	733	738
	Calc.[e]	185	526	544	566	557	584		
	Calc.[f]	142	338	534	556	563	689	733	743
	Exp.[g]	146		532	558	567		709	740
	Exp.[h]				553	568		738	
	Exp.[i]	145		533	561	570		735	742
	Exp.[j]			530	561	567		734	739
	Exp.[d]	144		534	560	569		737	744
AlN	This work	215	557	640	668	652	764	883	922
	Calc.[b]	236	553	629	649	631	717		
	Calc.[k]			619	677			893	918
	Calc.[l]			610	710				
	Calc.[e]	247	636	612	679	672	645		
	Exp.[m]	252		614	673	660		893	916
	Exp.[n]	241		607		660			924
	Exp.[i]			610	670				913
	Exp.[d]	248		614	673	660		894	917
BN	This work	447	918	988	1024	948	1179	1258	1286
	Calc.[k]			1006	1053			1258	1285

[a]Reference 28.
[b]Reference 14.
[c]Reference 19.
[d]Reference 9.
[e]Reference 16.
[f]Reference 17.
[g]Reference 1.
[h]Reference 4.
[i]Reference 6.
[j]Reference 7.
[k]Reference 18.
[l]Reference 15.
[m]Reference 2.
[n]Reference 3.

culated results with available experimental and a few *ab initio* results at the Γ point is made in Table III. We also compare, in Table IV, our results for GaN at the symmetry points *M*, *K*, and *A* with a recent *ab initio* work.[17] In this structure there are four atoms per unit cell, resulting in three acoustic and nine optical frequencies for any **q** point. The lowest three optical branches are found to be in the acoustic range. The other six optical branches are well separated from the acoustic as well as lower-lying optical branches for GaN and AlN. Thus there is an optical-optical gap in the phonon spectrum of GaN and AlN in the WZ structure, as opposed to the optical-acoustic gap in the ZB structure. There is no clear gap in the spectrum for BN, due to similarity of B and N masses.

The symmetry of atomic displacements at various symmetry points in the Brillouin zone for the WZ structure with space group C_{6v}^4 can be worked out by using group theoretical analysis.[27] Accordingly, atomic vibrations at the Γ point have the representations $1\times A_1+2\times B_1+1\times E_1+2\times E_2$. One A_1 and both E_1 are both Raman and infrared active, the E_2 modes are only Raman active, while B_1 modes are silent.

TABLE IV. The calculated phonon frequencies for wurtzite GaN at the *M*, *K*, and *A* points and their comparison with the *ab initio* calculations (Ref. 17). The mode degeneracy is indicated in parentheses. Units are cm^{-1}.

At *M* point		At *K* point		At *A* point	
This work	*Ab initio*	This work	*Ab initio*	This work	*Ab initio*
139(1*d*)	139(1*d*)	213(2*d*)	212(2*d*)	108(4*d*)	112(4*d*)
177(1*d*)	191(1*d*)	235(1*d*)	213(1*d*)	235(1*d*)	231(1*d*)
192(1*d*)	199(1*d*)	267(2*d*)	263(1*d*)	572(4*d*)	589(4*d*)
249(1*d*)	245(1*d*)	279(1*d*)	289(2*d*)	726(2*d*)	642(2*d*)
309(1*d*)	305(1*d*)	620(2*d*)	591(2*d*)		
320(1*d*)	316(1*d*)	620(2*d*)	633(1*d*)		
592(1*d*)	574(1*d*)	670(2*d*)	640(2*d*)		
596(1*d*)	579(1*d*)	677(1*d*)	684(1*d*)		
621(1*d*)	609(1*d*)				
645(1*d*)	633(1*d*)				
688(1*d*)	672(1*d*)				
716(1*d*)	697(1*d*)				

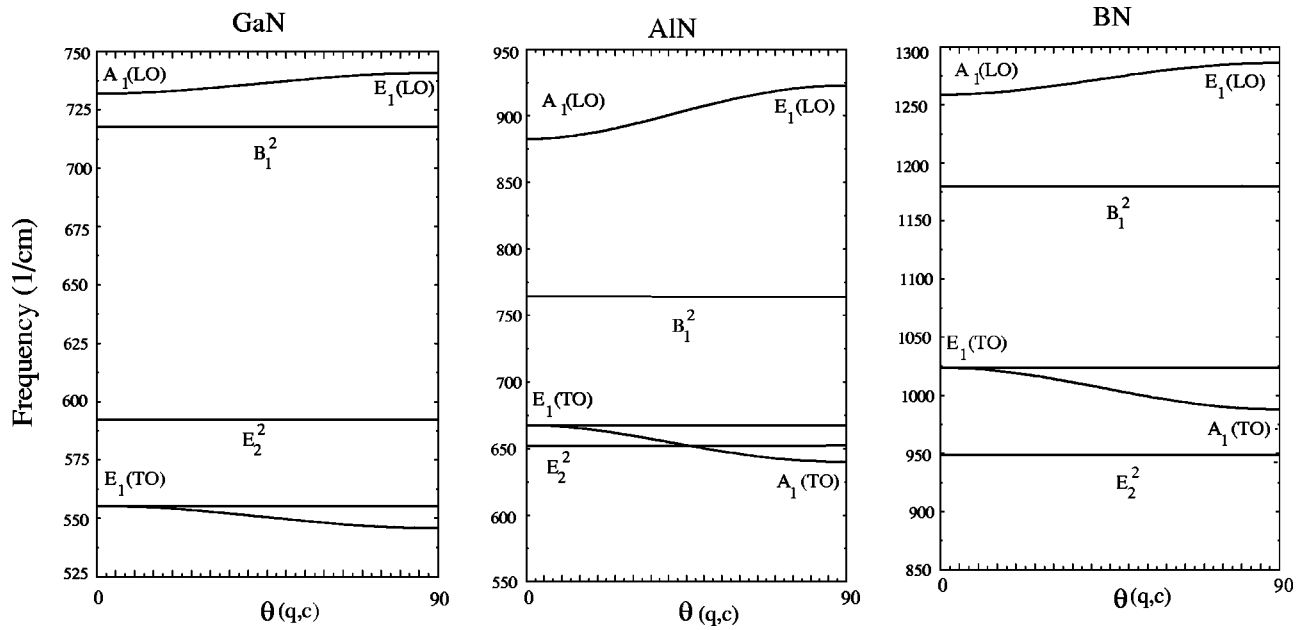

FIG. 3. Angular dependence of the optical-phonon modes in the wurtzite phase of AlN, GaN, and BN at Γ, with θ as the angle between the c axis and $\mathbf{q}\rightarrow 0$.

As a result of the anisotropy in the WZ structure, the transverse and longitudinal optical modes with representations A_1 and E_1 show an angular dependence for $\mathbf{q}\rightarrow 0$. Also, as a result of symmetry, at the A point in the Brillouin zone, longitudinal and transverse phonon modes become two- and fourfold degenerate, respectively, thus resulting in only four distinct phonon frequencies.

The vibrational characteristics of the WZ structure exhibit some changes from those of the ZB structure. The differences are linked to the differences in the two crystal structures. Although each atom is tetrahedrally bonded to four neighbors of another species in both the ZB and WZ structures, the connectivity of covalent bonds is different in the two structures. With reference to the middle of a straight bond along [111], one structure can be obtained by locally rotating the other by 60°. This leads to a difference in the connectivity of the second nearest neighbors in the two structures. The atomic coordinates within the primitive unit cell of the WZ structure are expressed in terms of an internal parameter u, which in the nonideal case of $u\neq\frac{3}{8}$ leads to two different bond lengths. Furthermore, some WZ materials are characterized by the ratio c/a_{hex} which is different from the ideal value of $\sqrt{8}/3$. We, however, have considered the experimental value of u and a_{hex}, and the ideal ratio $c/a_{hex}=\sqrt{8}/3$.

As a result of the geometrical differences between the two structures, we observe a few changes in the phonon spectrum and the density-of-states for the WZ phase compared with

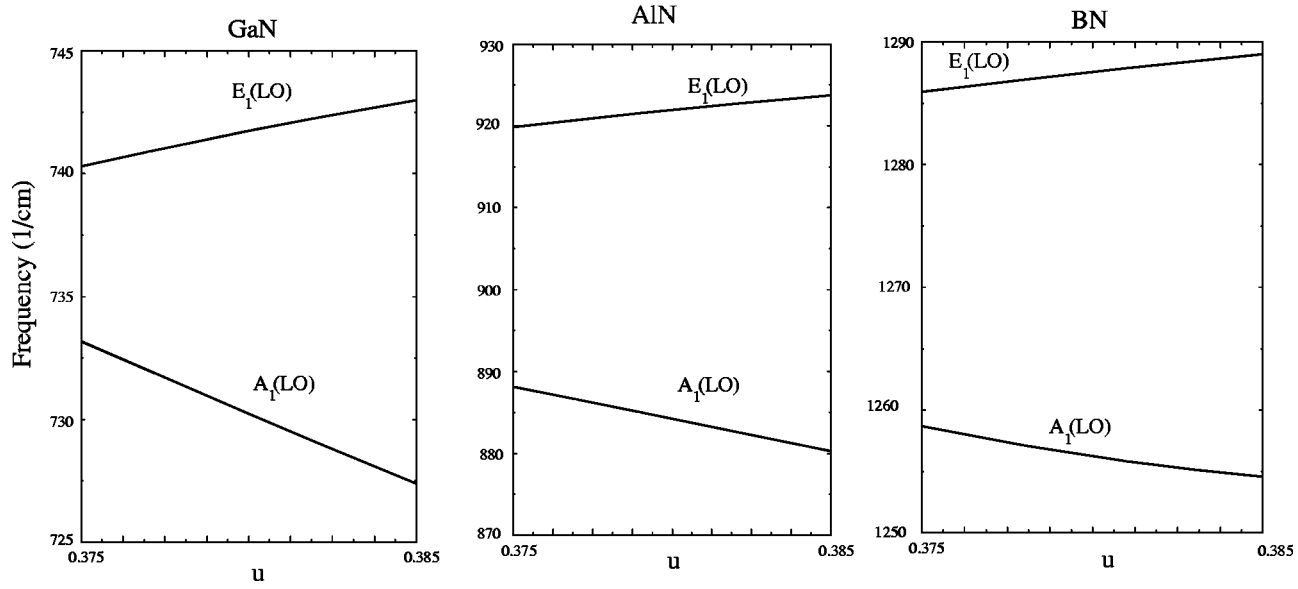

FIG. 4. Dependence of the A_1(LO) and E_1(LO) modes on the internal parameter u of the wurtzite structure.

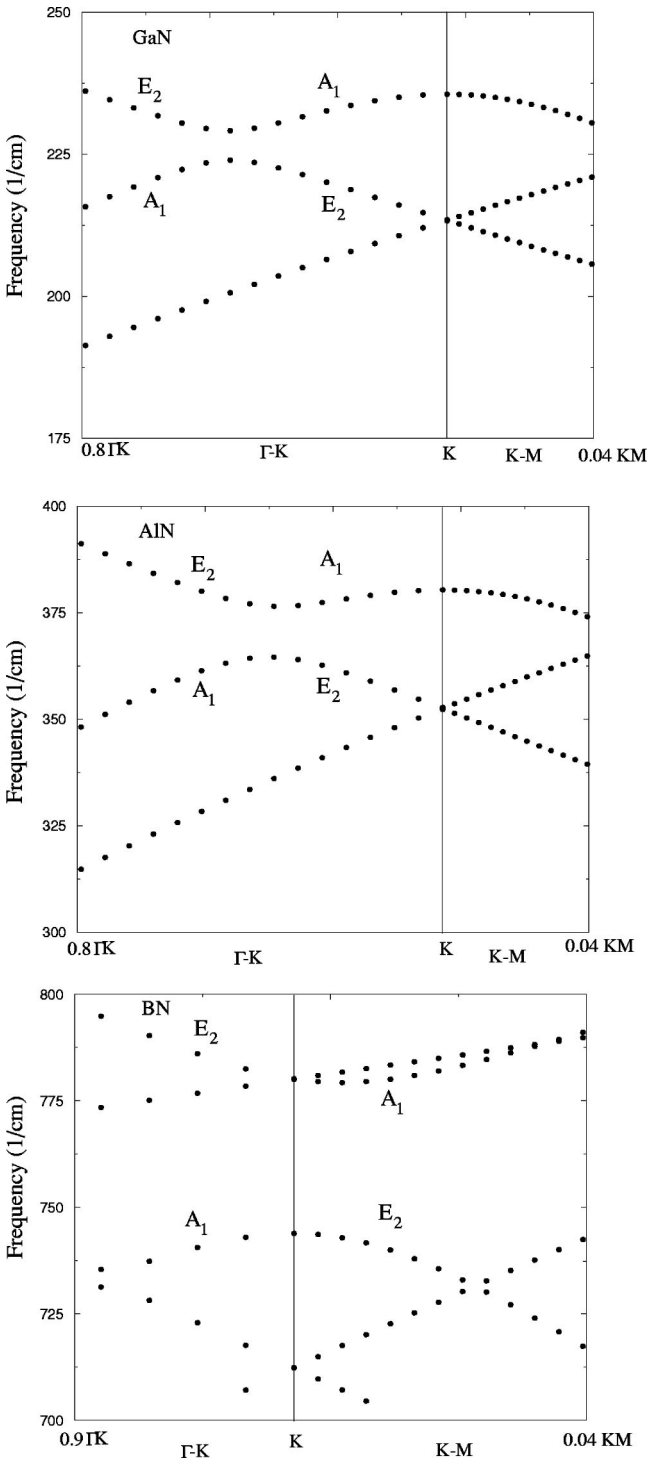

FIG. 5. The anticrossing effect between the A_1 acoustic and E_2 optical modes along the $\Gamma-K-M$ direction for the wurtzite structure.

the ZB phase. (i) As mentioned before, for the WZ phase there is no clear acoustic-optical separation. (ii) The extent of the BZ in the WZ phase along the [111] direction is only half of that in the ZB phase (i.e., ΓA in Fig. 2 is half as long as ΓL in Fig. 1). This leads to the *folding* of the ZB dispersion relation along $\Gamma-L$, with the results at L in ZB appearing at the Γ point in WZ. This is found to be the case within the numerical accuracy of our calculations. The density-of-states for AlN in the WZ phase shows the development of a small, but sharp, peak around 600 cm^{-1}, just below the large peak, which is also observed for the ZB phase. (iii) The angular variation of the optical modes for $\mathbf{q}\rightarrow 0$, due to the anisotropic nature of the WZ phase, is shown in Fig. 3. It is clear that only the A_1 and E_1 modes show this behavior. (iv) The separation between the E_1(LO) and A_1(LO) modes increases as the internal geometrical parameter u increases further from it ideal value of 0.375. This is shown in Fig. 4. This behavior can be readily understood in terms of the development of one long and three short bond lengths surrounding each atom in the WZ structure with a nonideal value of u. Similar behavior has also been seen in the *ab initio* work by Wagner and Bechstedt.[20] (v) Along $\Gamma-K-M$ in the Brillouin zone our results verify the anticrossing effect discussed in the work by Yu *et al.*[9] between the A_1 acoustic mode and the E_2 optical mode. As seen in Fig. 5 this effect takes place just before K along $\Gamma-K$ for GaN and AlN, and almost at the K point along $K-M$ for BN.

IV. SUMMARY

In this paper, we have applied an adiabatic bond-charge model to study the lattice dynamics of GaN, AlN, and BN in the zinc-blende and wurtzite structures. Our calculated phonon-dispersion curves for these materials are in very good agreement with the zone-center Raman measurements and available *ab initio* calculations. We have highlighted the main differences in the phonon spectra and density-of-states curves of these materials in the two phases. These include the angle dependence of optical-phonon modes, the effect of internal parameter on the A_1(LO) and E_1(LO) modes, and the anticrossing effect between the A_1 acoustic and E_2 optical modes in the wurtzite structure.

ACKNOWLEDGMENT

This work was supported by the Scientific and Technical Research Council of Turkey (TUBITAK).

[1] A. Gingolani, M. Ferrara, M. Lugara, and G. Scamario, Solid State Commun. **58**, 823 (1986).
[2] L. E. Neil, M. Grimsditch, and R. H. French, J. Am. Cerem. Soc. **76**, 1132 (1993).
[3] P. Perlin, A. Polian, and T. Suski, Phys. Rev. B **47**, 2874 (1993).
[4] M. Giehler, M. Ramsteiner, O. Brandt, H. Yang, and K. H. Ploog, Appl. Phys. Lett. **67**, 733 (1995).
[5] A. Tabata, R. Enderlein, J. R. Leite, S. W. da Silva, J. C. Glazerani, D. Schiroka, M. Kloidt, and K. Lischka, J. Appl. Phys. **79**, 4137 (1996).
[6] L. Filippidis, H. Siegle, A. Hoffmann, C. Thomsen, K. Karch, and F. Bechstedt, Phys. Status Solidi B **198**, 621 (1996).
[7] A. Cros, R. Dimitrov, H. Ambacher, M. Stutzmann, S. Christiansen, M. Albrecht, and H. P. Strunk, J. Cryst. Growth **181**, 197 (1997).
[8] H. Siegle, G. Kaczmarczyk, L. Filippidis, A. P. Litvinchuk, A. Hoffmann, and C. Thomsen, Phys. Rev. B **55**, 7000 (1997).
[9] V. Yu. Davydov, Yu. E. Kitaev, I. N. Goncharuk, A. N. Smirnov, J. Graul, O. Semchinova, D. Uffmann, M. B. Smirnov, A. P. Mirgorodsky, and R. A. Evarestov, Phys. Rev. B **58**, 12 899 (1998).
[10] G. Mirjalili, T. J. Parker, S. Farjami Shayesteh, M. M. Bülbül, S. R. P. Smith, T. S. Cheng, and C. T. Foxon, Phys. Rev. B **57**, 4656 (1998).
[11] D. Alexson, Leah Bergman, Mitra Dutta, K. W. Kim, S. Komirenko, Robert J. Nemanich, B.C. Lee, Micheal A. Stroscio, and SeGi Yu, Physica B **263-264**, 510 (1999).
[12] M. Schwoerer-Böning, T. Macrander, M. Pabst, and P. Pavone, Phys. Status Solidi B **215**, 177 (1999).
[13] J. Zi, X. Wan, G. Wei, K. Zhan, and X. Xie, J. Phys.: Condens. Matter **8**, 6323 (1996).
[14] I. Gorczyca, N. E. Christensen, E. L. Peltzer y Blancá, and C. O. Rodriguez, Phys. Rev. B **51**, 11 936 (1995).
[15] K. Kim, W. R. L. Lambrecht, and B. Segall, Phys. Rev. B **53**, 16 310 (1996).
[16] K. Shimada, T. Sota, and K. Suzuki, J. Appl. Phys. **84**, 4951 (1998).
[17] K. Parlinski and Y. Kawazoe, Phys. Rev. B **60**, 15 511 (1999).
[18] K. Karch and F. Bechstedt, Phys. Rev. B **56**, 7404 (1997).
[19] K. Karch, J.M. Wagner, and F. Bechstedt, Phys. Rev. B **57**, 7043 (1998).
[20] J.-M. Wagner and F. Bechstedt, Phys. Status Solidi B **216**, 793 (1999).
[21] C. Bungaro, K. Rapcewicz, and J. Bernholc, Phys. Rev. B **61**, 6720 (2000).
[22] W. Weber, Phys. Rev. Lett. **33**, 371 (1974); Phys. Rev. B **15**, 4789 (1977); K. C. Rustagi and W. Weber, Solid State Commun. **18**, 673 (1979); T. Azuhata, T. Sota, and K. Suzuki, J. Phys.: Condens. Matter **7**, 1949 (1995); B. D. Rajput and D. A. Browne, Phys. Rev. B **53**, 9052 (1996).
[23] P. Santini, L. Miglio, G. Benedek, U. Harten, P. Ruggerone, and J. P. Toennies, Phys. Rev. B **42**, 11 942 (1990); H. M. Tütüncü, S. J. Jenkins, and G. P. Srivastava, *ibid.* **56**, 4656 (1997); H. M. Tütüncü and G. P. Srivastava, *ibid.* **59**, 4925 (1999); H. M. Tütüncü and G. P. Srivastava, *ibid.* **57**, 3791 (1998).
[24] S. Yip and Y. C. Chang, Phys. Rev. B **30**, 7037 (1984); K. Lambert and G. P. Srivastava, Phys. Rev. B **56**, 13 387 (1997).
[25] A. Wright and J. Nelson, Phys. Rev. B **50**, 2159 (1994); **51**, 7866 (1995).
[26] G. L. Doll, in *Properties of Group III Nitrides*, edited by J. H. Edgar (INSPEC, IEE, London, 1994).
[27] S. C. Miller and W. F. Love, *Tables of Irreducible Representations of Space Groups and Corepresentations of Magnetic Space Groups* (Pruett, Boulder, 1967).
[28] K. Miwa and A. Fukumoto, Phys. Rev. B **48**, 7897 (1993).